POLITECNICO
MILANO 1863

SCUOLA DI INGEGNERIA INDUSTRIALE
E DELL'INFORMAZIONE

Executive Summary of the Thesis

Rotorcraft Ground Resonance using Lyapunov Characteristic Exponents estimated from Multibody Simulation

Laurea Magistrale in Aeronautical Engineering - Ingegneria Aeronautica

Author: Gianni Cassoni

Advisor: Prof. Pierangelo Masarati

Academic year: 2021-2022

1. Introduction

Helicopter ground resonance is a phenomenon that may develop when a helicopter has an imbalance in the axis of rotation of the hub and is spinning near or on the ground. This type of instability can lead to the destruction of the structure and injuries to the crew, in a modern helicopter, this occurs rarely but still is one of the more dangerous situations that can lead to the complete loss of the aircraft. The use of linearized equations of motion has been shown to produce very accurate frequency predictions, but the damping has proven much more difficult to predict. This is particularly true for rotor systems that include elastomeric lag dampers, which exhibit highly nonlinear response characteristics.

2. Hammond model of ground resonance

To understand the ground resonance a classical model, which became a de-facto benchmark, was proposed by Hammond in a seminal 1974 paper [2]. A sketch is presented in Fig. 1. The model is a simplified system of the hub and blades coupling, there exits another model i.e. Kunz [3], in which a damper is made inoperative to obtain the effect of self-excited vibrations.

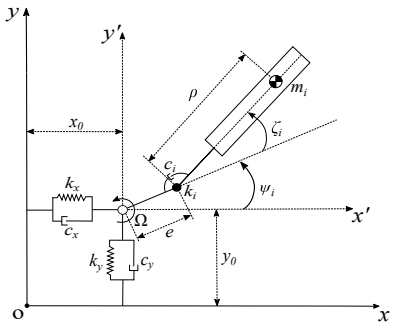

Figure 1: Hammond model from [2].

The data of the model are presented in Table **??**. The equations of motion of the system without the assumption of small Lead-Lag angle (*ad-hoc* model), are thus

$$\begin{aligned} &I_b\ddot{\zeta}_i - f_i(\dot{\zeta}_i) + k_i\zeta_i + e\Omega^2 S_b \sin\zeta_i \\ &- S_b[\ddot{x}_h \sin(\psi_i + \zeta_i) - \\ &\ddot{y}_h \cos(\psi_i + \zeta_i)] = 0 \quad i = 1 \dots N_b \end{aligned} \tag{1}$$

for each blade, where $f_i(\dot{\zeta}_i)$ is the blade damping moment, with $f_i(\dot{\zeta}_i) = -c_i\dot{\zeta}_i$ when the linear

damper of [2] is considered, and

$$(m_x + N_b m_b)\ddot{x}_h + c_x\dot{x}_h + k_x x_h \tag{2a}$$
$$- S_b \sum_{i=1}^{N_b} [\ddot{\zeta}_i \sin(\psi_i + \zeta_i) + (\Omega +$$
$$\dot{\zeta}_i)^2 \cos(\psi_i + \zeta_i) + \frac{e\Omega^2}{\rho}\cos\psi_i] = 0$$
$$(m_y + N_b m_b)\ddot{y}_h + c_y\dot{y}_h + k_y y_h \tag{2b}$$
$$- S_b \sum_{i=1}^{N_b} [\ddot{\zeta}_i \cos(\psi_i + \zeta_i) - (\Omega +$$
$$\dot{\zeta}_i)^2 \sin(\psi_i + \zeta_i) - \frac{e\Omega^2}{\rho}\sin\psi_i] = 0$$

with $\rho = S_b/m_b$, for the airframe. The numerical data proposed in [2] are reported in Table **??**.

3. Lyapunov Characteristic Exponents

Lyapunov Characteristic Exponents (LCEs) are used for the analysis of stability of non linear dynamical system. From the Oseledec Multiplicative Ergodic Theorem [5] states that the following limit exists

$$\Lambda^{\pm}(t) = \lim_{t\to\pm\infty} \frac{1}{2t} \log([\mathbf{Y}^{\dagger}(t, t_0)\mathbf{Y}(t, t_0)]) \tag{3}$$

or can be written in the following form

$$\lambda_i = \lim_{t\to\infty} \frac{1}{t} \log(\frac{||\mathbf{Y}(t, t_0) \cdot \vec{w}_i(t_0)||}{||\vec{w}_i(t_0)||}) \tag{4}$$

Where $\vec{w}$ is the deviator vector and $\mathbf{Y}(t, t_0)$ is the State Transition Matrix. From the limit with the QR method [4] is possible to obtain all the LCEs.

4. LCEs of the Hammond model

To study the stability of the Nonlinear, time-periodic model LCEs approach is used. The first case with all Lead-Lag Dampers operative is presented in Fig. 2. The second case with one Lead-Lag Damper inoperative (the third Lead-Lag Damper) is presented in Fig. 3. As expected the first case with all Lead-Lag Dampers operative converges to the one obtained by Hammond [2]. For the second case, a different result is obtained in the instability region, the LCEs show that the solution after a transient region converges to a stable limit cycle so thus the first LCE converges to zero.

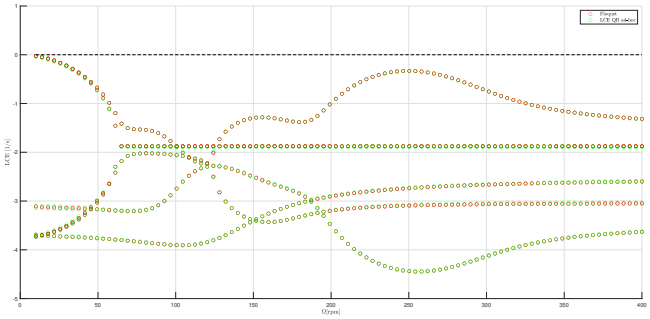

Figure 2: LCE of isotropic case.

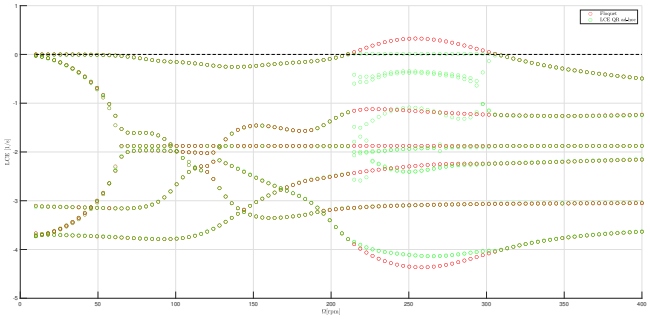

Figure 3: LCE of non-isotropic case.

The LCEs spectrum is local and depends on the initial value of the system. For all the calculations an initial value of $x_0 = 0.1[m]$ is used. The Fig. 3 show that as expected the instability region is a limit cycle and the interval follows the Floquet results.

5. Maximum LCE

In most applications it can be useful just to estimate the Maximal LCE, Rosenstein algorithm [7] is able to estimate the MLCE just from a short time series. Let a time series the trajectory, $\mathbf{X}$, can be reconstructed using the time delay method. The reconstructed trajectory can be expressed as a matrix where each row is a phase-space vector. That is,

$$\mathbf{X} = [\mathbf{X}_1, \mathbf{X}_2, ..., \mathbf{X}_m] \tag{5}$$

For an N-point time series, $\{x_1, x_2, ..., x_N\}$, each $\mathbf{X}_k$ is given by

$$\mathbf{X}_k = [x_{1+(k-1)J}, x_{2+(k-1)J}, ..., x_{M+(k-1)J}]^T \tag{6}$$

where $k = 1, ..., m$.
Thus, $\mathbf{X}$ is an $M \times m$ matrix, and the constants m, M, J, and N are related as

$$M = N - (m-1)J \tag{7}$$

where m is the embedding dimension, N length of the time series and J the reconstruction delay.
The embedding dimension is usually estimated in accordance with Takens' theorem, i.e. $m > 2n$.
After reconstructing the dynamics, the algorithm locates the nearest neighbor of each point on the trajectory. The nearest neighbor, $\mathbf{X}_{\hat{j}}$, is found by searching for the point that minimizes the distance to the particular reference point, $\mathbf{X}_j$. This is expressed as

$$d_j(0) = \min_{\mathbf{X}_{\hat{j}}} ||\mathbf{X}_j - \mathbf{X}_{\hat{j}}|| \tag{8}$$

where $d_j(0)$ is the initial distance from the j^{th} point to its nearest neighbor, and $||..||$ denotes the Euclidean norm. Also an additional constraint is that nearest neighbors have a temporal separation greater than the mean period ($\bar{T}$) (the reciprocal of the mean frequency of the power spectrum, although it can be expected that any comparable estimate, e.g., using the median frequency of the magnitude spectrum, yield equivalent results) of the time series:

$$|j - \hat{j}| > \bar{T} \tag{9}$$

This allows to consider each pair of neighbors as nearby initial conditions for different trajectories. The largest Lyapunov exponent is then estimated as the mean rate of separation of the nearest neighbors.
The j^{th} pair of nearest neighbors diverge approximately at a rate given by the largest Lyapunov exponent:

$$d_j(i) \approx C_j e^{\lambda_1 (i\Delta t)} \tag{10}$$

where C_j is the initial separation.
By taking the logarithm of both sides

$$\ln d_j(i) \approx \ln C_j + \lambda_1 (i\Delta t) \tag{11}$$

a set of approximately parallel lines (for $j = 1, 2, ..., M$), each with a slope roughly proportional to λ_1. The largest Lyapunov exponent is calculated using a least-squares fit to the "average" line defined by

$$y(i) = \frac{1}{\Delta t} \langle \ln d_j(i) \rangle \tag{12}$$

where $\langle .. \rangle$ denotes the average over all values of j.

6. MLCE of the MBDyn model

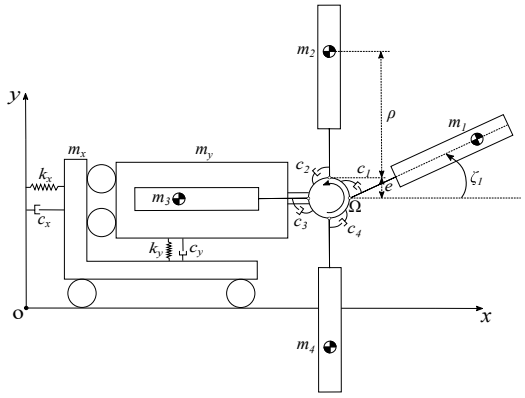

Figure 4: Sketch of the MBDyn model of Hammond's system [2].

One application of the Maximum LCE method (5) is to study the stability of time series. By using MBDyn is possible to obtain the time evolution of a more complex model, to validate the method Hammond model is recreated using the MBDyn environment. However, owing to the peculiar modeling characteristics of the solver, the different equivalent inertia terms of the airframe respectively associated with motion in the x and y directions have been obtained by splitting the airframe into two parts:

- the first part is connected to the ground by a constraint that only allows its absolute displacement in the x direction;
- the second part is connected to the first one by a constraint that only allows its displacement relative to the first one in the y direction.

The mass of the second part is m_y, whereas that of the first one is $m_x - m_y$, such that the overall mass associated with the absolute motion of the hub center in the x direction is m_x.
The first part is connected to the ground by a spring and a damper, of characteristics k_x and c_x. Another spring and damper, of characteristics k_y and c_y, connect the second to the first part.

The rotor hub is modeled as a third, massless part, whose relative motion with respect to the second part of the airframe is a prescribed rotation about axis z with constant rpm.
The blades are described as rigid bodies through their absolute displacement and orientation, constrained to the hub by revolute joints that only allow their relative rotation about the lead-lag hinge, whose axis is parallel to the global z axis, and thus to the axis of rotation of the rotor. Such rotation is restrained by an angular damper that represents the equivalent lead-lag damper torque. A sketch of the model is shown in Fig. 4.

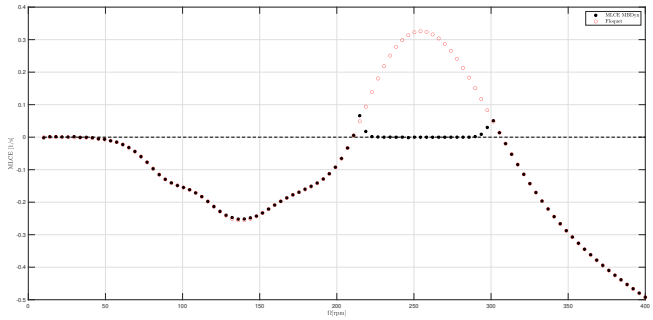

Figure 5: estimated MLCE of non-isotropic case, using Jacobian-less method.

The results of Fig. 5 show that with the MLCE method is possible to obtain the maximum LCE and thus is possible to evaluate the stability/instability of the system. The results follow the one obtained in section 4. As a comparison the Fig. 7 for the non-isotropic case with one damper inoperative and Fig. 6 for the isotropic one.

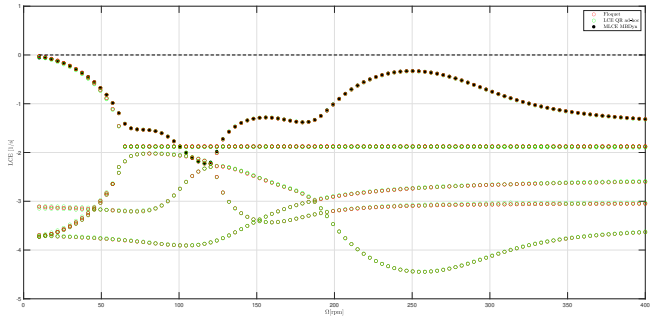

Figure 6: LCE of isotropic case.

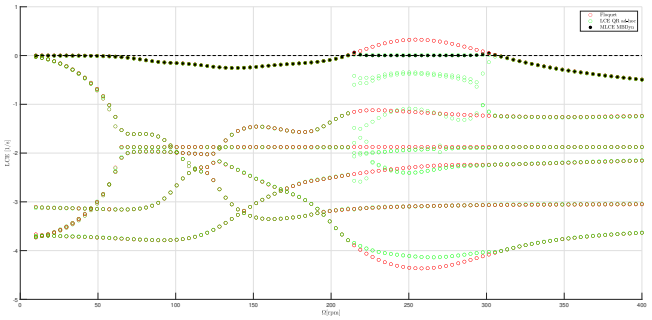

Figure 7: LCE of non-isotropic case.

7. The Inter-Blade Lead-Lag Damper model

A different approach to reduce the instability is presented [1], the use of a different configuration for the Lead-Lag Damper, one of the solutions proposed is the inter-blade damper (7.1) and another one is the Inter-2-Blade damper (7.2).

7.1. Inter-Blade Lead-Lag Damper

For the inter-blade Lead-Lag Damper configuration the equations of motion of the *ad-hoc* in the x-direction (2a) and y-direction (2b) remain unchanged. The main difference is thus in the blades equation as follows

$$\begin{aligned} &I_b\ddot{\zeta}_i - f_i(\dot{\zeta}_i, \dot{\zeta}_{i+1}, \dot{\zeta}_{i-1}) + k_i\zeta_i + e\Omega^2 S_b \sin\zeta_i \\ &- S_b[\ddot{x}_h \sin(\psi_i + \zeta_i) \\ &- \ddot{y}_h \cos(\psi_i + \zeta_i)] = 0 \quad i = 1 \dots N_b \end{aligned} \tag{13}$$

for each blade, where $f_i(\dot{\zeta}_i, \dot{\zeta}_{i+1}, \dot{\zeta}_{i-1})$ is the blade damping moment, with $f_i(\dot{\zeta}_i, \dot{\zeta}_{i+1}, \dot{\zeta}_{i-1}) = -\frac{c_i}{2}(\dot{\zeta}_i - \dot{\zeta}_{i-1}) - \frac{c_i}{2}(\dot{\zeta}_i - \dot{\zeta}_{i+1})$ when the linear damper of [2] is considered, and the same as equation as before. The numerical data proposed in [2] are reported in Table **??**.

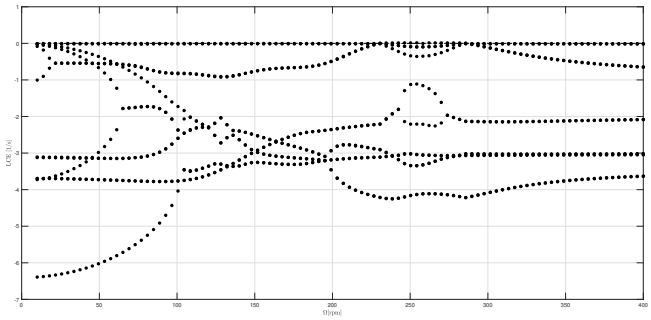

Figure 8: LCEs of Inter-Blade Damper configuration with the third damper inoperative.

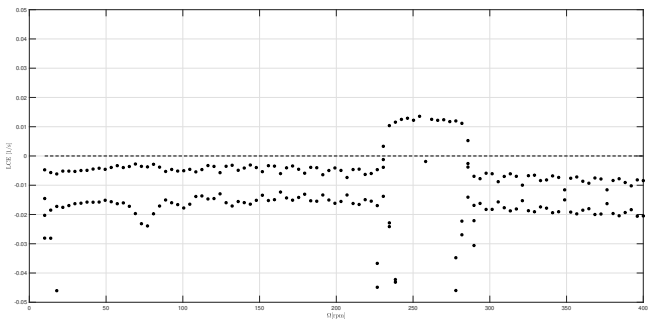

Figure 9: LCEs of Inter-Blade Damper configuration with the third damper inoperative, enlargement of the unstable LCEs.

7.2. Inter-2-Blade Lead-Lag Damper

For the Inter-2-Blade Lead-Lag Damper configuration the equations of motion of the *ad-hoc* in the x direction (2a) and y direction (2b) remain unchanged. The main difference is thus in the blades equation as follows

$$\begin{aligned} &I_b\ddot{\zeta}_i - f_i(\dot{\zeta}_i, \dot{\zeta}_{i-2}, \dot{\zeta}_{i+2}) + k_i\zeta_i + e\Omega^2 S_b \sin\zeta_i \\ &- S_b[\ddot{x}_h \sin(\psi_i + \zeta_i) \\ &- \ddot{y}_h \cos(\psi_i + \zeta_i)] = 0 \quad i = 1 \dots N_b \end{aligned} \tag{14}$$

for each blade, where $f_i(\dot{\zeta}_i, \dot{\zeta}_{i-2}, \dot{\zeta}_{i+2})$ is the blade damping moment, with $f_i(\dot{\zeta}_i, \dot{\zeta}_{i-2}, \dot{\zeta}_{i+2}) = -\frac{c_i}{4}(\dot{\zeta}_i - \dot{\zeta}_{i-2}) - \frac{c_i}{4}(\dot{\zeta}_i - \dot{\zeta}_{i+2})$ when the linear damper of [2] is considered, and the same as equation as before. The numerical data proposed in [2] are reported in Table **??**.

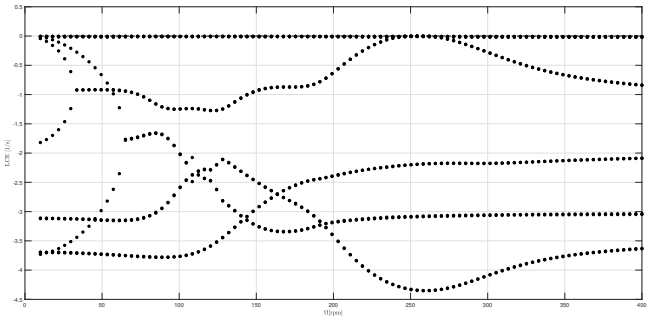

Figure 10: LCEs of Inter-2-Blade Damper configuration with the third damper inoperative.

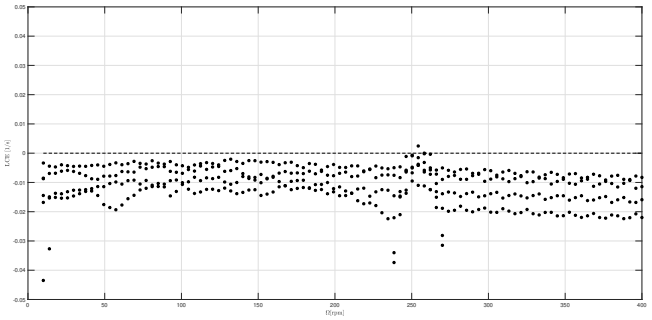

Figure 11: LCEs of Inter-2-Blade Damper configuration with the third damper inoperative, enlargement of the unstable LCEs.

8. Hammond model with non linear dampers

The case of a more realistic damper model, characterized by a nonlinear constitutive law studied in [8], is considered. The equations of motion of the *ad-hoc* in the x hub direction (2a) and y hub direction (2b) remain unchanged. The main difference is thus in the blades equation as follows

$$\begin{aligned} &I_b\ddot{\xi}_i + f_{di} + k_i\xi_i + e\Omega^2 S_b sin(\xi_i) \qquad (15)\\ &- S_b[\ddot{x}_h \sin(\psi_i + \xi_i) - \\ &\ddot{y}_h \cos(\psi_i + \xi_i)] = 0 \quad i = 1, ..., N \qquad (16) \end{aligned}$$

where

$$f_{di} = \begin{cases} \chi\dot{\xi}_i|\dot{\xi}_i| + C_L\dot{\xi}_i & |\dot{\xi}_i| < |\dot{\xi}_L| \\ \bar{\chi}\dot{\xi}_L|\dot{\xi}_L| & |\dot{\xi}_i| \geq |\dot{\xi}_L| \end{cases} \tag{17}$$

with $\chi = \bar{\chi} - C_L\dot{\xi}_L$ and $\bar{\chi} = 1.2203 \times 10^6$ $[N \cdot m \cdot s^2/rad^2]$, $\dot{\xi}_L = 1.0[deg/s]$, $C_L = c_i$.

8.1. All Lead-Lag Dampers operative

In the first case study, the condition is that all Lead-Lag dampers are operative with different

initial conditions of the third blade angular velocity. This is because of the nonlinear law of the damper after a threshold is saturated. So by showing that the solution reaches a limit cycle if the initial condition is higher than the level of saturation is possible to have ground resonance even if all the dampers are operative.

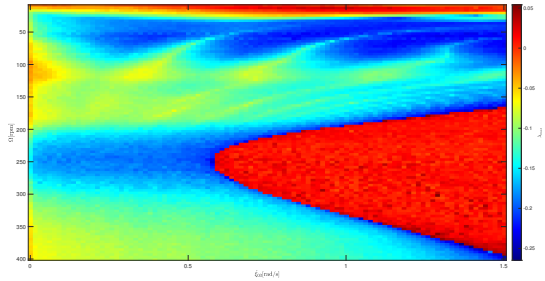

Figure 12: MLCE with different inital condition of $\dot{\xi}_{03}$.

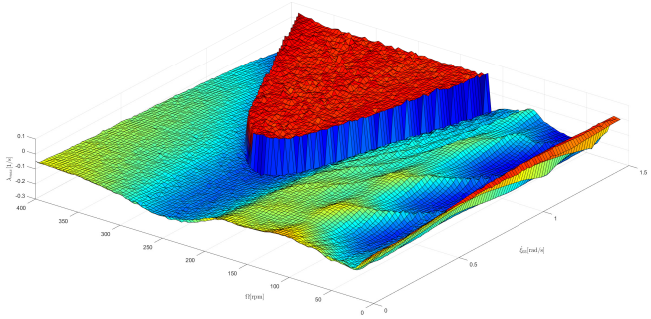

Figure 13: 3D plot of the MLCE with different inital condition of $\dot{\xi}_{03}$.

8.2. One Lead-Lag Damper inoperative

In this case study, the condition is that the third Lead-Lag damper is inoperative with different initial conditions of the third blade angular velocity. This is because in the non-linear law of the damper after a threshold is saturated. So by showing that the solution reaches a limit cycle if the initial condition is higher than the level of saturation is possible to have ground resonance even if all the dampers are operative. One damper is inoperative, with the different initial conditions, after a value, the damper is already saturated.

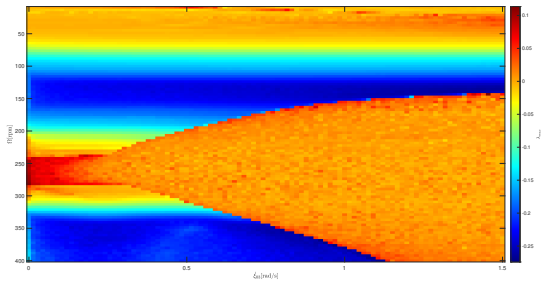

Figure 14: MLCE with the third damper inoperative and different inital condition of $\dot{\xi}_{03}$.

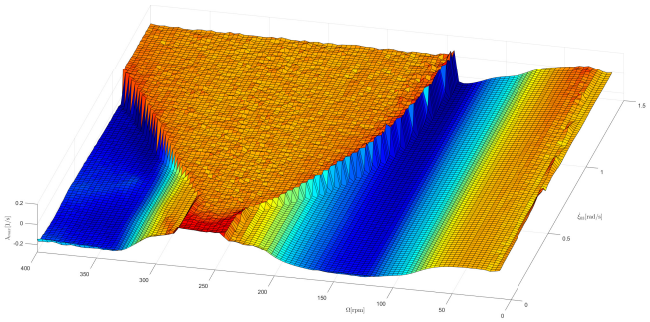

Figure 15: 3D plot of the MLCE with the third damper inoperative and different inital condition of $\dot{\xi}_{03}$.

8.3. MLCE at fixed rpm for one Lead-Lag Damper inoperative

The results presented in [8] in terms of LCEs are here reproduced and presented in Fig. 16, considering the *ad-hoc* model, which includes the geometric nonlinearities associated with the finite motion of the parts, and the multibody model, which on top of that adds the formulation of the blade motion concerning the absolute reference frame, in form of a set of differential-algebraic equations (DAEs). The two analyses show essentially identical results since the resulting time histories are quite similar. The parametric stability of the isotropic problem at fixed rpm is then studied by varying the linear contribution in Eq. (17), namely the term $-C_L\dot{\zeta}_i$, with $C_L \in [0, c_i]$, as proposed in [8], after the insurgence of a limit cycle for $C_L = 0$ was observed in [6].

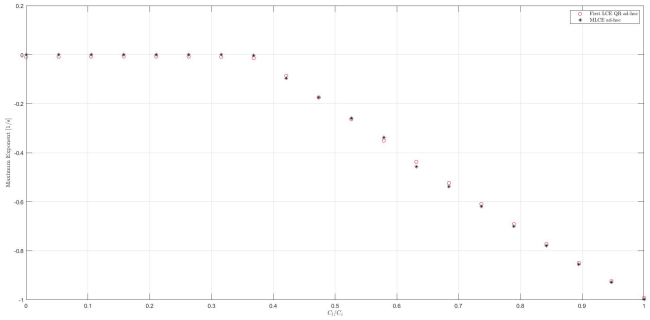

Figure 16: MLCE of isotropic case with nonlinear *ad-hoc* model and nonlinear damper, using discrete QR and Jacobian-less method.

9. Conclusions

The use of LCEs the Ground Resonance, Fig. 3, shows that the method gives an accurate indication of the type of dynamical instability that occurs in a limit cycle. The LCEs method also was implemented for more complex cases as for the Inter-Blade Lead-Lag configuration (subsection 7.1) and the Inter-2-Blade Lead-Lag configuration (subsection 7.2). The method's strength is that can provide a stability analysis even for systems that don't have periodicity or are strong non-linear where Floquet fails. The drawbacks are the computational cost of performing this type of analysis this is because to have an accurate estimate of the time series a longer one is needed and the problem also scales with the degrees of freedom very quickly. A way to make a stability analysis more computational advantage is by only computing the MLCE (subsection 5) with this method also the knowledge of the Jacobian matrix is no longer necessary, for this reason, it was implemented in MBDyn (section 6). One drawback of the method is the necessity of estimating some parameters a priory, i.e. the embedding dimension and the time delay. Then the method was applied to a more complex system to show the potential application in the MBDyn environment. This thesis's main objective was to show the LCEs and MLCE's possible application in multibody dynamics with a focus on the ground resonance problem.

References

[1] L. Frison, A. Zanoni, and P. Masarati. The inter-2-blade lead-lag damper concept. Fort Worth, TX, USA, May 20-22 2022.

[2] C. Eugene Hammond. An application of Floquet theory to prediction of mechanical instability. *Journal of the American Helicopter Society*, 19(4):14–23, 1974. doi:10.4050/JAHS.19.14.

[3] Donald Kunz. Nonlinear analysis of helicopter ground resonance. *Nonlinear Analysis: Real World Applications*, 3:383–395, 09 2002.

[4] Pierangelo Masarati. Estimation of lyapunov exponents from multibody dynamics in differential-algebraic form. *Proceedings of the Institution of Mechanical Engineers, Part K: Journal of Multi-body Dynamics*, 227:23–33, 03 2013.

[5] Mark Pollicott. *References*, page 155–160. London Mathematical Society Lecture Note Series. Cambridge University Press, 1993.

[6] Giuseppe Quaranta, Vincenzo Muscarello, and Pierangelo Masarati. Lead-lag damper robustness analysis for helicopter ground resonance. *Journal of Guidance Control and Dynamics*, 36:1150–1161, 2013.

[7] Michael T. Rosenstein, James J. Collins, and Carlo J. De Luca. A practical method for calculating largest lyapunov exponents from small data sets. *Physica D: Nonlinear Phenomena*, 65(1):117–134, 1993.

[8] Aykut Tamer and Pierangelo Masarati. Stability of nonlinear, time-dependent rotorcraft systems using lyapunov characteristic exponents. *Journal of the American Helicopter Society*, 61, 04 2016.